Structural Investigation of Langmuir and Langmuir−Blodgett Monolayers of Semifluorinated Alkanes

Patrycja Dynarowicz Łatka,*,‡ Marta Pérez-Morales,† Eulogia Muñoz,† Marcin Broniatowski,‡ María T. Martín-Romero,† and Luis Camacho*,†

Departamento de Química Física y Termodinámica Aplicada, Universidad de Córdoba, Campus Universitario de Rabanales, Ed. Marie Curie, E-14071 Córdoba, Spain, and Faculty of Chemistry, Jagiellonian University, Ingardena 3, 30-060 Kraków, Poland

Received: December 13, 2005; In Final Form: February 8, 2006

The behavior of a semi-fluorinated alkane ($C_{10}F_{21}C_{19}H_{39}$) has been studied at the air−water interface by using surface pressure and surface potential−area isotherms as well as infrared spectroscopy for the Langmuir−Blodgett films. In addition, based on the quantum chemical PM3 semiempirical approach, the dimer structure was investigated, and the double helix was found to be the most stable conformation of the dimer. The obtained results allow us to imply that the phase transition observed in the course of the surface pressure/area isotherm is due to a conformational change originating from the double helix to a vertical, single helix configuration.

Introduction

Semifluorinated alkanes (SFAs, $C_nF_{2n+1}C_mH_{m+1}$, abbr. F*n*H*m*) have been found to form stable Langmuir monolayers, as it was initially shown by Gaines,[1] despite the lack of any polar headgroup. The structure of a floating SFA monolayer at the air−water interface or a film transferred on freshly cleaved mica or cleaned silicon wafers still remains a topic of debate, and different structural models have been proposed on the basis of atomic force microscopy (AFM), X-ray reflectivity, and grazing-incidence small-angle X-ray scattering (GISAXS) measurements.[2−8] The model of a homogeneous film structure, where molecules are oriented either parallel to each other[2] or in a head-to-tail configuration,[7] has been suggested. However, such models neither provide a satisfactory interpretation of the diffraction data nor explain the formation of surface hemimicelles,[3−6] ribbons, as well as nanospirals. In such structures, the fluorinated segments are vertically oriented with respect to the interface while the hydrocarbon chains are in contact with the water/solid support, tilted and partially disordered.[8]

Such a particular organization of a SFA monolayer originates not from the lack of any polar group, but is due to the presence of a fluorinated segment. In fact, semifluorinated alkanoic acids spontaneously form monodispersed nanometric clusters of a form and size similar to those formed by SFA.[9,10] The formation of nanometric structures has been related either to cluster formation upon spreading (nucleation and growth mechanism) or to the spinodal decomposition during the rapid evaporation of the spreading solvent.[9,10] Other amphiphilic molecules have been reported to form clusters of sizes similar to SFAs that fuse upon compression, forming a uniform monolayer. However, for monolayers from SFAs, the clusters remain separated and do not fuse even under high surface pressures.

To get a deeper insight into the molecular architecture of SFAs spread at the air/water interface, we apply herein different physicochemical methods to those mentioned above (AFM, GISAXS), such as surface pressure together with electric surface potential measurements in addition to FTIR spectroscopy for LB films. These methods are based on different physical phenomena as compared to modern optical methods and provide supplementary details on the molecular level, which are not accessible from other techniques. For our investigations, we have chosen F10H19 as a representative of SFAs, due to its good film-forming abilities and high monolayer stability, at least at low surface pressures.[11]

Previously, surface pressure−area and surface potential−area isotherms for a number of SFAs belonging to different homologous series were studied,[11−13] and it appeared that SFAs containing more than six carbon atoms in the hydrogenated moiety exhibited a phase transition between two liquid or liquid-condensed phases at about 5 mN/m. These phases have been related to smectic ordering of SFAs in bulk.[14] Interestingly, one of the recent contributions shows that semifluorinated alkanols exhibit a phase transition similar to that of SFAs.[15]

Experimental Section

Materials. The semifluorinated alkane F10H19 used in this research was synthesized according to the procedure described elsewhere.[11] Perfluorodecyl iodide (98%) was purchased from Fluorochem, while nonadecene (99%) was supplied by Aldrich. Both reagents were used as received. The crude semifluorinated alkane was purified by subsequent crystallizations from hexane (spectroscopy grade, Aldrich). Its final purity was greater than 99%, which was proved by ^{1}H and ^{13}C NMR spectra, mass spectrometry, DSC analysis, IR spectra, as well as elemental analysis (Anal. Calcd for F10H19: C, 44.28; H, 5.00. Found: C, 44.41; H, 4.93).

The spreading solutions for Langmuir experiments were prepared by dissolving the investigated SFA in chloroform (Aldrich, spectroscopy grade) with a typical concentration of ca. 0.5 mg/μL. The solution was dropped onto a water surface with a Hamilton microsyringe, precise to $\pm$0.2 μL. Ultrapure water (produced by a Millipore Milli-Q unit, pretreated by a Millipore reverse osmosis system (resistivity = 18.2 MΩ cm))

* To whom correspondence should be addressed. Phone: +34 957 21 86 17. Fax: +34 957 21 86 18. E-mail: qf1cadel@uco.es.
† Universidad de Córdoba.
‡ Jagiellonian University.

10.1021/jp057270u CCC: $33.50
Published on Web 03/07/2006

was used as a subphase. The subphase temperature was 21 °C and pH = 5.7.

Methods. Langmuir monolayer experiments were carried out with a NIMA 601 trough (Coventry, U.K.) (total area = 600 cm^2), equipped with two symmetrical barriers placed on an antivibration table. Surface pressure was measured with the accuracy of ±0.1 mN/m, using a Wilhelmy plate made from chromatography paper (Wharman Chr1) as a pressure sensor. After being spread, the monolayers were left for 10 min for the solvent to evaporate, after which the compression process was initiated with a barrier speed of 10−20 cm^2/min.

F10H19 monolayers were transferred upon withdrawing of the solid substrate through the interface covered with the SFA film with the speed of 3−5 mm/min. The transfer ratio, $\tau = A_I/A_S$ (wherein A_I is the change in the monolayer area during the transfer and A_S is the area of the solid substrate covered by monolayer), was close to 1 in all of the cases. Tests of multilayers assemblies by sequential monolayer transfer, that is, withdrawal (↑) and immersion (↓) of the substrate through the interface, were unsuccessful, as the second film transferred upon the immersion was detached during the withdrawal. The monolayers were transferred onto CaF_2 substrates (transparent to IR radiation), which were cleaned before several times with $CHCl_3$ (to eliminate organic impurities) and rinsed out with ultrapure water.

FTIR measurements were performed on a Mattson Research Series instrument equipped with a DTGS detector. The background spectrum of an uncoated CaF_2 substrate was recorded as the reference. The FTIR transmission spectra of the films were measured with and without polarized light (s and p), under different incidence angles, to estimate the average tilt of the hydrocarbon and the fluorinated segment of the chain with respect to the normal surface.

Semiempirical PM3 methods implemented in the HyperChem molecular modeling package (version 6)[16] were used for global geometrical optimization of F10H19 monomer and dimer, following the procedure described elsewhere.[15] A RMS (root-mean-square) gradient of 0.003 kcal/(Å·mol), which indicates the first derivative of total energy with respect to the displacement of each atom in any direction, was taken as convergence criteria for geometrical optimization.

Results

Surface Pressure and Surface Potential/Area Isotherms. The surface pressure/area ($\pi-A$) isotherm of F10H19 has already been described.[11] Figure 1a (solid line) shows the compression of a F10H19 monolayer.

Stability studies were performed by monitoring the relaxation area for different constant surface pressures, $\pi_{constant}$. At $\pi_{constant} \leq 14$ mN/m, the loss of area was negligible after 1 h.

Figure 1a (dashed line) presents the compression modulus (reciprocal of compressibility, defined as $C_s^{-1} = -A(d\pi/dA)$), which clearly shows the characteristic transition in the SFA monolayer between liquid and liquid-condensed states as well as the lack of a solid phase, as described elsewhere.[11,12] Such phases, designed by phases I and II (see Figure 1a), have been related to the smectic order of the SFAs in bulk.[14] The maximum values of the compression modulus are $C_s^{-1} \approx 92$ mN/m (at $\pi = 2.4$ mN/m and $A = 0.37$ nm^2), and $C_s^{-1} \approx 140$ mN/m (at $\pi = 10.7$ mN/m and $A = 0.33$ nm^2) for phases I and II, respectively.

The change in surface potential, ΔV, was recorded simultaneously with the decrease of the area of the film (solid line in Figure 1b). For our calculations, we have applied the Helmholtz equation[17] in the form

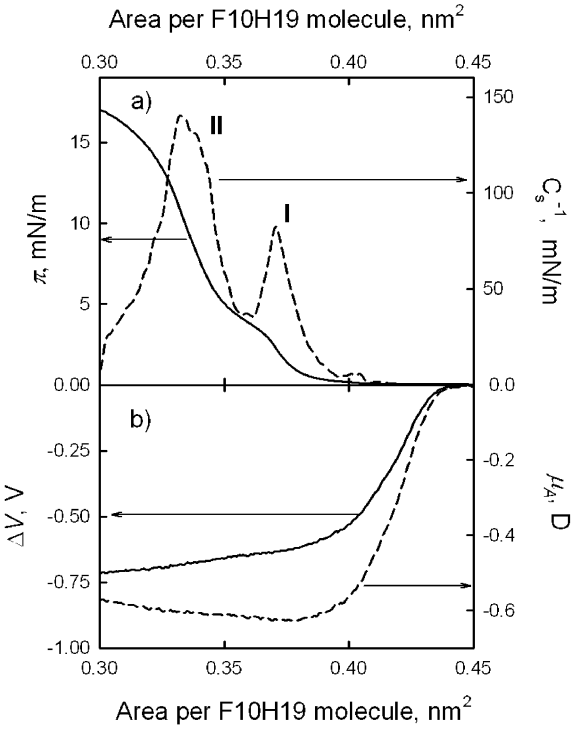

Figure 1. (a) $\pi-$Area (A) isotherm (solid line) and compression modulus (C_s^{-1}) versus A (dashed line) of F10H19 under compression from 0 to 17 mN/m. (b) $\Delta V-A$ isotherm (solid line) and apparent dipole moment (μ_A) versus A (dashed line) under compression from 0 to 17 mN/m.

$$\Delta V = \frac{\langle \mu_z \rangle}{A \epsilon \epsilon_0} \tag{1}$$

where $\langle \mu_z \rangle$ is the effective dipole moment or the average vertical component of the molecular dipole moment, $\vec{\mu}$, ϵ_0 is the vacuum permittivity, and ϵ is the relative dielectric permittivity of the monolayer. The apparent dipole moment, μ_A, is defined as:

$$\mu_A = \Delta V \cdot A \cdot \epsilon_0 = \frac{\langle \mu_z \rangle}{\epsilon} \tag{2}$$

The plots μ_A-A are presented in Figure 1b (dashed line). As it can be seen, the apparent dipole moment decreases upon compression, reaching its minimum, $\mu_A = -0.63$ D, at a molecular area close to the first maximum of the compression modulus ($A = 0.37$ nm^2). This μ_A value can be related to phase I. The transition between phases I and II is observed in the μ_A-A plots as a slow increase of the apparent dipole moment up to $\mu_A = -0.59$ D at $A = 0.33$ nm^2 (value related to phase II).

FTIR Spectroscopy of F10H19 LB Monolayers. In Figure 2, the FTIR spectra corresponding to one monolayer of F10H19 transferred onto CaF_2 at $\pi = 4$ mN/m (a), 7 mN/m (b), and 10 mN/m (c) are shown. As a reference, the FTIR spectrum of F10H19 in a KBr pellet (d) is also presented. The main band positions and assignments are provided in Table 1. In the spectra, the symmetric and antisymmetric stretching vibrations of the CH_2 ($\nu_a(CH_2) = 2920$ and $\nu_s(CH_2) = 2850$ cm^{-1}) and CF_2 ($\nu_a(CF_2) = 1215$ and $\nu_s(CF_2) = 1151$ cm^{-1}) groups can be clearly recognized. These four bands have similar relative intensity for both LB films (Figure 2a−c) and in the pellet spectrum (Figure

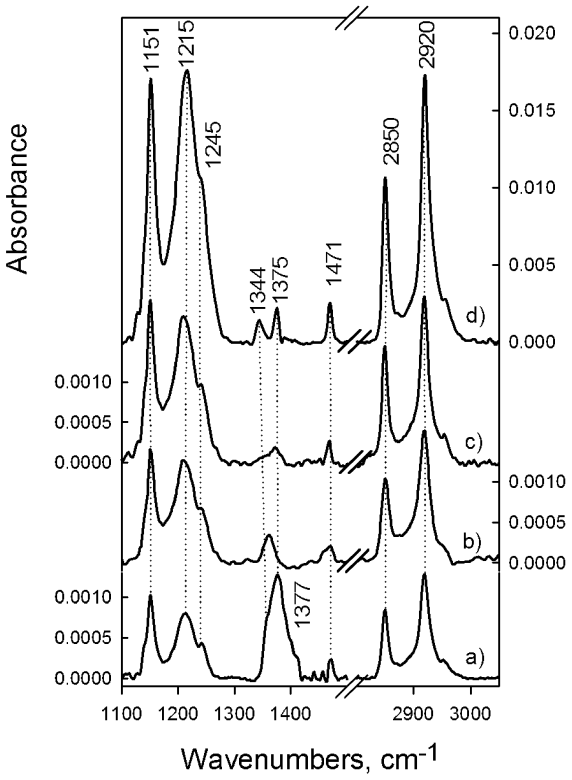

Figure 2. FTIR transmission spectra of one monolayer of F10H19 transferred on both sides of a CaF_2 substrate at $\pi = 4$ mN/m (a), 7 mN/m (b), and 10 mN/m (c). As reference, the spectrum of $F_{10}H_{19}$ in a KBr pellet (d) is also shown.

2d), which suggests, in a qualitative way, that the hydrocarbon chain and the fluorinated moiety have similar relative tilts in the LB films.

As it was described in the bibliography,[18−30] the band positions of the $\nu(CH_2)$ modes (antisymmetric and symmetric) can reveal the structural state of the alkyl chains. Thus, values ≤ 2920 cm^{-1} and ≤ 2850 cm^{-1} for $\nu_{as}(CH_2)$ and $\nu_s(CH_2)$ modes, respectively, should correspond to a crystalline state, while band positions at 2928 and 2856 cm^{-1} for those vibrating modes, respectively, are characteristic for a liquid state. Likewise, the full width at half-maximum (fwhm) of the $\nu_{as}(CH_2)$ mode has been used to provide the ad-layer order.[20,25,31,32] Thus, a bandwidth narrower than 20 cm^{-1} has been related to a crystalline state, while a broader peak corresponds to a disordered liquid state. Consequently, the wavenumbers and the fwhm values obtained for the pellet and for the LB films at different pressures (see Table 1) prove ordered structures of the alkyl chains.

Additional information about the hydrogenated segment can be inferred from the scissor band of the CH_2 group ($\delta(CH_2)$). The wavenumbers and the fwhm of this band have been related to the packing of the alkyl chains.[18,33] For triclinic packing, a strong, sharp, and narrow singlet band at 1474−1470 cm^{-1}, for hexagonal packing, a relatively broader singlet at 1469−1468 cm^{-1}, for amorphous, a broad band around 1465 cm^{-1}, and for orthorhombic packing, a two-bands split, are observed. The singlet band at 1471 ± 1 cm^{-1}, with a fwhm of 9−10 cm^{-1} indicates a pseudotriclinic subcell packing.

The small bands observed at 1344 and 1375 cm^{-1} in the pellet spectrum (Figure 2d) are assigned to $\nu(CF_3)$ modes.[33,34] Indeed, these bands were also observed, with a similar relative intensity and wavenumber, for F4H20 and F8H20 pellet spectra (data not shown). However, the strong band observed at 1377 cm^{-1} together with the shoulder near 1350 cm^{-1}, for the $\pi = 4$mN/m spectrum (Figure 2a), have been identified as "axial CF_2" stretching vibrations, which originated from the activation of bands from the inside of the Brillouin zone of the infinite fluorocarbon helix, due to the finite length of the CF_2 sequence.[35,36] Strong bands near 1340 and 1375 cm^{-1} are observed for semifluorinated alkanethiols monolayers (SAM) on Au.[36,37] These bands were also found for perfluorocarbon oligomers, except for poly(tetrafluoroethylene),[37] as well as in the LB film of fluorinated fatty acids.[38] The small bands observed in the 1344−1375 cm^{-1} region for the LB films transferred at 7 and 10 mN/m (Figure 2b,c) could be assigned to $\nu(CF_3)$ modes, even though we cannot discard a small contribution of the axial CF_2. In a similar way, the 1377 cm^{-1} band of the $\pi = 4$mN/m LB film spectrum should also have a small contribution of the $\nu(CF_3)$ modes.

To estimate the average tilt of the hydrocarbon and the fluorinated segment with respect to the normal surface, spectra under polarized light, s and p, and at different incidence angles were measured for monolayers transferred at $\pi = 4$ and 10 mN/m. Previously, spectra under normal incidence and different polarization angles were determined, being coincident in all cases. This fact allows us to discard the anisotropy of the LB films in the *xy* plane (support plane).[39]

Figure 3 shows the spectra for $\pi = 4$ mN/m (a) and $\pi = 10$ mN/m (b) under s (solid lines)- and p (dotted line)-polarized light and 60° incidence. The predominant band for s and p spectra at $\pi = 4$ mN/m corresponds to the axial CF_2 stretching vibrations, as it appears under normal incidence (Figure 2a). For the $\pi = 10$ mN/m spectrum, the 1374 cm^{-1} band is not the most predominant. In the nonpolarized (Figure 2c) and p-polarized (Figure 3b, dotted line) spectra, this band should mainly be assigned to the $\nu(CF_3)$ modes. However, for the s spectrum (Figure 3b, solid line), the shape of this band suggests a mixing of the axial CF_2 and $\nu(CF_3)$ modes. The intensity of the $\nu_a(CH_2)$, $\nu_s(CH_2)$, $\nu_a(CF_2)$, and $\nu_s(CF_2)$ modes has been interpreted using the dichroic ratio $Dr = A_s/A_p$, where A_s and A_p are the absorption under s- and p-polarized light, respectively. According to Vandevyver et al.,[39,40] for very thin films:

$$Dr = \frac{A_s}{A_p} \approx \left(\frac{n_1\cos(r) + n_3\cos(i)}{n_1\cos(i) + n_3\cos(r)}\right) \times \left(\frac{2{n_1}^3 n_3 \sin(i)^2}{{n_2}^4}\frac{\langle\cos(\omega)^2\rangle}{\langle\sin(\omega)^2\rangle} + \cos(i)\cos(r)\right)^{-1} \quad (3)$$

where n_1 (=1), n_2, and n_3 (=1.41) are the refractive index of air, film, and CaF_2, respectively; $r = \arcsin[n_1 \sin(i)/n_3]$ is obtained from the Snell ratio; i and ω are the incident angle and the angle of the transition dipole with respect to the normal; and brackets stand for average values. According to eq 3, with $i = 60°$ and $\omega = 90°$, and taking $n_2 = 1.36$,[36] the value of *Dr* was calculated to be 2.35, while for $i = 60°$ and $\omega = 54.7°$ (random orientation), one obtains $Dr = 1.32$.

Table 2 shows the range of the dichroic ratio, *Dr*, obtained for $\nu_s(CH_2)$ and $\nu_a(CH_2)$ bands (hydrogenated segment) and for $\nu_s(CF_2)$ and $\nu_a(CF_2)$ (fluorinated segment) in four different experiments. This table also complies ω values determined from *Dr* and eq 3 as well as the tilt of the fluorinated and hydrogenated segments with respect to the support ($\theta = 90° - \omega$). In fact, the vibrations of these stretching $\nu(CF_2)$ and $\nu(CH_2)$ modes are in the plane of F−C−F and H−C−H atoms, respectively, and therefore the alkyl chains should be close to normal with respect to the plane of the stretching vibrations.

TABLE 1: Band Position Assignments and Wavelength Half Widths (fwhm) of the FTIR Transmission Spectra

	LB, $\pi = 4$ mN/m		LB, $\pi = 7$ and 10 mN/m		pellet	
mode description	position cm^{-1}	fwhm cm^{-1}	position cm^{-1}	fwhm cm^{-1}	position cm^{-1}	fwhm cm^{-1}
$\nu_a(CH_2)$	2920	18	2920	17	2919	16
$\nu_s(CH_2)$	2851	12	2850	12	2850	11
$\delta(CH_2)$	1471	9	1470	9	1471	10
axial CF_2	1377[a]					
$\nu(CF_3)$			1374[b]		1375	
$\nu(CF_3)$			1348[b]		1344	
$\nu_a(CF_2)$	1244		1245		1244	
$\nu_a(CF_2)$	1214	36	1212	44	1215	40
$\nu_s(CF_2)$	1152	15	1152	16	1153	16

[a] The $\nu(CF_3)$ mode contributes to this band. [b] Corresponding to the $\pi = 10$ mN/m spectrum. The contribution of the axial CF_2 mode to these bands cannot be discarded.

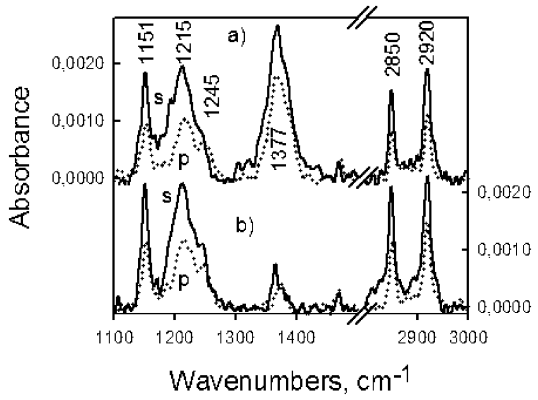

Figure 3. FTIR transmission spectra of one monolayer of F10H19 transferred on both sides of a CaF_2 substrate at $\pi = 4$ mN/m (a) and $\pi = 10$ mN/m (b) under s (solid lines)- and p (dotted lines)-polarized light and 60° incidence.

TABLE 2: Average Dichroic Ratio, *D*, Angles between the Incidence Polarized Light and the Transition Dipole, ω, and Chain Tilt with Respect to the Support, θ, for $\nu_s(CH_2)$ and $\nu_a(CH_2)$ Bands (Hydrogenated Segment) and for $\nu_s(CF_2)$ and $\nu_a(CF_2)$ Bands (Fluorinated Segment)

		LB, $\pi = 4$ mN/m (phase I)	LB, $\pi = 10$ mN/m (phase II)
$\nu_s(CF_2)$	Dr	1.9−1.8	2.1−1.8
and	ω	68° ± 2°	71° ± 4°
$\nu_a(CF_2)$	$\theta = 90° - \omega$	22° ± 2°	19° ± 4°
$\nu_s(CH_2)$	Dr	1.9−1.7	1.85−1.65
and	ω	66° ± 3°	65° ± 3°
$\nu_a(CH_2)$	$\theta = 90° - \omega$	24° ± 3°	25° ± 3°

As it can be seen in Table 2, the tilt, θ, of the hydrogenated and fluorinated segments is similar for both transfer pressures; for example, for the fluorinated segment the tilt changes from 22° ± 2° at $\pi = 4$ mN/m to 19° ± 4° when $\pi = 10$ mN/m.

Semiempirical PM3 Geometrical Optimization of the Monomer and Dimer Structures. Quantum chemical, ab initio calculations offer a way to obtain detailed information on intermolecular aggregates. However, an approximate description of intermolecular interactions may be done by using one of the semiempirical methods, for example, PM3 approximation.[15] The results obtained from the global geometrical optimization of the F10H19 monomer show a vertical arrangement of the carbon backbone, in which the perfluorinated fragment adopts a helical configuration (see Scheme 1a). For the fluorinated segment, the C−F bond length, CCC and FCC angles, and torsion angles found herein are coincident with those reported by Vysotsky et al.,[15] for the $C_8F_{17}CH_2CH_2OH$ molecule.

SCHEME 1: Molecular Geometries of the Most Stable Monomer (a) and Dimer (b) of F10H19[a]

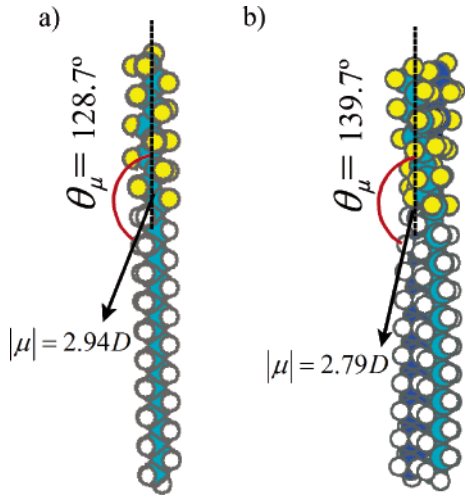

[a] θ_μ is the tilt of the dipole moment vector with respect to the axis of the carbon backbone (monomer), and with respect to the helix axis (dimer). For the dimer, the C atoms of each molecule are differently colored for a better display.

Because the van der Waals radius of the fluorine atom is larger than one-half of the C−C distance, steric hindrance causes the chain to adopt a 15/7 helical conformation, which makes the carbon backbone more rigid and enlarges the chain's cross-sectional area.[41] The standard enthalpy of formation obtained from the PM3 calculations for the optimized structure of F10H19 monomer (Scheme 1a) was found to be $\Delta H_1 = -4767.9$ kJ/mol.

The dimer formation was studied using a procedure similar to that described elsewhere.[15] The molecular geometry of the most stable dimer is shown in Scheme 1b (where the C atoms of each molecule are differently colored for a better display). The self-organization of molecules results in the formation of a partial double helix, where the monomer helix has similar winding. The formation of a complete double helix requires the presence of 34 carbon atoms in the fluorinated segment.[15] Supposing that the double helix axis is vertically oriented with respect to the interface, the cross section of the dimer was estimated to be 0.76 nm^2, approximately 0.38 nm^2 per molecule. The latter value agrees with the mean molecular area associated with phase I. The standard enthalpy of formation obtained for the structure presented in Scheme 1b was $\Delta H_2 = -9749.1$ kJ/mol. Thus, the dimerization enthalpy equals: $\Delta H_D = \Delta H_2 - 2\Delta H_1 = -213.3$ kJ/mol. In any case, other quasi-equilibrium configurations of the dimer can be obtained with thermodynamic

characteristics similar to the structure of Scheme 1b. For example, for a dimer with a parallel configuration of the chains, the dimerization enthalpy close to $\Delta H_D \approx -200.0$ kJ/mol is obtained, although such a value depends on the relative orientation of each molecule. Although the formation of trimers, tetramers, or clusters of high number has not been analyzed, it was proved that, for fluoroalkanols, the tetramer consists of two interacting dimers.[15]

Discussion

Similar tilts of the hydrogenated and fluorinated segments in the F10H19 molecule (~19−25°, Table 2) for $\pi = 4$ mN/m (phase I) and $\pi = 10$ mN/m (phase II) obtained from FTIR spectra are surprising due to a different area per molecule associated with both phases, $A_I = 0.37$ nm^2 and $A_{II} = 0.33$ nm^2 for phases I and II, respectively. In fact, assuming that only the fluorinated segment controls the surface area, and using the value $\theta_{II} \approx 19°$ (Table 2) for the average tilt of F10H19 in phase II, from geometrical considerations, the tilt angle for phase I should be $\theta_I = \arccos[A_{II} \cos(\theta_{II})/A_I] = 33°$, which differs from the value obtained experimentally ($\theta_I \approx 22°$, see Table 2).

A strong band at 1377 cm^{-1} in the LB spectrum of the monolayer transferred at $\pi = 4$ mN/m (phase I, Figure 2a), corresponding to the CF_2 vibrations along the fluorocarbon helix,[35,36] does not appear in the spectra of the monolayers transferred at $\pi = 7$ and 10 mN/m (phase II, Figure 2b,c)) and must be related to a predominant helical configuration in phase I versus phase II. In fact, the 1377 cm^{-1} band is the prevalent band when only phase I exists. Thus, this band appears with a similar intensity in the spectra realized for monolayers transferred at $\pi = 2$ mN/m (data not shown). When phase II is formed (for $\pi \geq 5$ mN/m), the intensity of the bands in the 1377 cm^{-1} region decreases abruptly. In this case, the observed bands must be related to the $\nu(CF_3)$ mode, even though a small contribution of the axial CF_2 mode cannot be discarded. Moreover, it points out that perfluorinated oligomers[37] are the only that exhibit this band (1377 cm^{-1}), and therefore the presence of that axial band in the spectrum of phase I can be taken as additional proof of the existence of the double helix. This fact enables us to put forward the hypothesis that the I to II phase transition observed in the surface pressure/area isotherm (see Figure 1a) is due to the conformational change originated from the double helix (Scheme 1b) to a vertical, single helix configuration (Scheme 1a).

Based on a quantum chemistry semiempirical approach, a similar hypothesis was proposed by Vysotsky et al.,[15] for C_8F_{17}-CH_2CH_2OH monolayers. By applying a similar procedure, we have found that the most stable dimer of the F10H19 molecules has the structure of a partial double helix.

The model of the double helix configuration at low surface pressure region may explain the formation of nanospiral structures observed by Moeller et al.[8] for F14H20 monolayers. In fact, different spirals in the scanning force microscopy (SFM) images of monomolecular layers of this compound were detected, both right- and left-handed, showing no preference in chirality. However, the double helix dimer could be formed in two different ways with equal and opposite directions of the helixes winding.[15] Therefore, this suggests that the dimers, or the high order aggregate with double helix configuration, are the origin of the nanospiral structures. Other authors[4,5] observed circular structures for different F*n*H*m* compounds. For these cases, it was demonstrated that the original spirals were transformed by the lateral compression into circular-hexagonal objects.[8]

Previous studies suggest that the F10H19 hydrogenated segment is weakly ordered in a liquidlike state,[8,11] due to a different cross section of the hydrogenated (~0.20 nm^2) and fluorinated (~0.28 nm^2) segments. However, the dichroic ratio obtained by using polarized-light FTIR spectroscopy indicates a nearly crystalline ordered structure of the hydrogenated alkyl chains, and a similar tilt for the hydrogenated and fluorinated segments, which agree with the prediction of the PM3 semiempirical calculation, where the hydrogenated tail participates in the dimer enthalpy formation and a similar tilt is obtained for both segments.

Moreover, the double helix configuration for phase I allows us to explain two additional atypical phenomena observed in the surface behavior of SFAs:

(a) It explains that, despite F10H19 molecules having a similar tilt in phases I and II, they occupy larger areas in phase I (~0.37 nm^2) than in phase II (~0.33 nm^2). In that respect, the increase of the average twist of the F−C−F bonding due to the double helix formation is relatively small. Thus, if the 360° twist is completed for 34 carbon atoms,[15] the average contribution for each F−C−F bound can be estimated to be 360/34 = 10.5° only, a value smaller than the experimental one (22° for phase I, see Table 2).

(b) It also explains why the absolute value of the apparent dipole moment in phase I ($|\mu_A| = 0.63$ D) is higher than that in phase II ($|\mu_A| = 0.59$ D), despite a similar (or, more precisely, slightly more vertical) molecular tilt in phase II with respect to phase I. This behavior of the apparent dipole moment is generally found for the majority of SFAs, where it is possible to observe the decrease of $|\mu_A|$ in the vicinity of collapse.[11−13] Langmuir monolayers of classical amphiphilic molecules containing hydrophilic headgroups undergo strong anchoring into the water surface. However, this is not the case of F*n*H*m* molecules, because the hydrophilic headgroups are missing. In this case, the surface potential ΔV of the monolayer can be related to the dipole moment of the molecule through the Helmholtz formula (eqs 1 and 2).

As evidenced by IR spectroscopy, the films are isotropic in the $x-y$ (support) plane. Therefore, the average vertical component of the dipole moment, $\langle \mu_z \rangle$ can be expressed by:

$$\langle \mu_z \rangle = |\vec{\mu}| \cos(\theta) \cos(\theta_\mu) \qquad (4)$$

where θ is the average chain tilt with respect to the support (assuming that the hydrogenated and fluorinated segments have approximately a similar tilt), and θ_μ is the tilt of the dipole moment vector with respect to the axis of the carbon backbone in the case of the monomer (see Scheme 1a), and with respect to the helix axis for the dimer (see Scheme 1b).

The approximate dipole moments for monomer and dimer (see Scheme 1) have been estimated from geometrical optimization by using PM3 methods. In Scheme 1, the arrows indicate the direction of the dipole moment obtained. For the monomer, we obtain $|\vec{\mu}| = 2.94$ D, $\theta_\mu = 128.7°$, and $\theta \approx 22°$ (average angle between the hydrogenated and fluorinated segments, see Table 2), and therefore $\langle \mu_z \rangle_{\text{phase II}} = -1.7$ D. For the dimer case, $|\vec{\mu}| = 2.79$ D (per molecule), $\theta_\mu = 139.7°$, and $\theta \approx 23°$, and therefore $\langle \mu_z \rangle_{\text{phase I}} = -1.95$ D. Thus, although the absolute dipole moment value per molecule is lower for the partial double helix dimer configuration (phase I), its vertical component is higher than that for the monomer (phase II). From eq 2, it can be obtained that:

$$|\mu_A|_{\text{phase I}} = \frac{1.95}{\epsilon} D > |\mu_A|_{\text{phase II}} = \frac{1.7}{\epsilon} D \qquad (5)$$

Values of ϵ ranging from 2 to 4.5 have been previously used for SFAs.[42,43] A good agreement between the value predicted by eq 5 and the experimental one can be obtained for $\epsilon \approx 3$. Thus, by using this value and eq 5, the following values $|\mu_A|_{\text{phase I}} = 0.65$ D and $|\mu_A|_{\text{phase II}} = 0.57$ D have been calculated, versus the experimental values 0.63 and 0.59 D, respectively. This, however, can only be considered as a qualitative comparison, because different approximations have been used. Therefore, the double to single helix transition can explain the decrease of the absolute value of the dipole moment through the I to II phase transition observed along the $\pi-A$ isotherm (see Figure 1b).

Conclusions

The results obtained with FTIR prove a similar tilt angle ($\sim$19−25°) for the hydrogenated and fluorinated segments in F10H19 molecules, being independent of the monolayer transfer pressure. Moreover, the presence of a strong band at 1377 cm^{-1} in the $\pi = 4$ mN/m spectrum (phase I), related to the CF_2 vibrations along the fluorocarbon helix,[35,36] is missing in the $\pi = 7$ and 10 mN/m spectra (phase II). This fact enables us to put forward a hypothesis that the I to II phase transition observed in the surface pressure/area isotherm (see Figure 1a) is due to the conformational change originated from the double helix to a vertical configuration (single helix). The dimerization with a double helix conformation at the air−water interface has already been suggested, on the basis of theoretical considerations, for semifluorinated alkanols.[15]

This hypothesis permits us to explain the peculiar surface behavior of SFAs molecules. Thus, the larger area per molecule as well as a higher absolute value of the apparent dipole moment for phase I with respect to phase II (besides the similar tilt angle of the fluorinated segment in both phases) explain a double helix formation in phase I. Moreover, the results from semiempirical PM3 global geometrical optimization of the F10H19 dimer show the formation of a partial double helix being the most stable structure, wherein the monomer helix has a similar winding. In this way, the double helix dimer can be formed in two different ways: with equal and opposite directions of helices winding.[15] This phenomenon allows one to explain the formation of nanospirals structures, with both right- and left-handed winding, observed for F14H20 by Moeller et al.[8]

Acknowledgment. We thank the Spanish CICYT for financial support of this research in the framework of Project BQU2001-1792. Also, we thank the Ministerio de Ciencia y Tecnología for the contract for one of the authors (Ramón y Cajal Program). P.D.-Ł thanks Junta de Andalucía for the travel grant.

References and Notes

(1) Gaines, G. L. *Langmuir* **1991**, *7*, 3054.
(2) Huang, Z.; Acero, A. A.; Lei, N.; Rice, S. A.; Zhang, Z.; Schlossman, M. C. *J. Chem. Soc., Faraday Trans.* **1996**, *94*, 545.
(3) Krafft, M. P.; Giulieri, F.; Fontaine, P.; Goldmann, M. *Langmuir* **2001**, *17*, 6577.
(4) Maaloum, M.; Muller, P.; Krafft, M. P. *Angew. Chem., Int. Ed.* **2002**, *41*, 4331.
(5) Zhang, G.; Maaloum, M.; Muller, P.; Benoit, N.; Krafft, M. P. *Phys. Chem. Chem. Phys.* **2004**, *6*, 1566.
(6) Fontaine, P.; Goldmann, M.; Faure, M. C.; Konovalov, O.; Muller, P.; Krafft, M. P. *J. Am. Chem. Soc.* **2005**, *127*, 512.
(7) El Abed, A.; Pouzet, E.; Faure, M. C.; Saniere, M.; Abillon, O. *Phys. Rev. E* **2000**, *62*, R5895.
(8) Mourran, A.; Tartsch, B.; Gallyamov, M.; Magonov, S.; Lambreva, D.; Ostrovskii, B. I.; Dolbnya, I. P.; de Jeu, W. H.; Moeller, M. *Langmuir* **2005**, *21*, 2308.
(9) Kato, T.; Kameyama, M.; Kawano, M. *Thin Solid Films* **1996**, *273*, 232.
(10) Kato, T.; Kameyama, M.; Ehara, M.; Iimura, K. *Langmuir* **1998**, *14*, 1786.
(11) Broniatowski, M.; Sanchez Macho, I.; Miñones, J.; Dynarowicz-Ł tka, P. *J. Phys. Chem. B* **2004**, *108*, 13403.
(12) Broniatowski, M.; Miñones, J.; Dynarowicz-Ł tka, P. *J. Colloid Interface Sci.* **2004**, *279*, 552.
(13) Broniatowski, M.; Sanchez Macho, I.; Miñones, J.; Dynarowicz-Ł tka, P. *Appl. Surf. Sci.* **2005**, *246*, 342.
(14) Broniatowski, M.; Dynarowicz-Ł tka, P.; Witko, W. *J. Fluorine Chem.* **2005**, *126*, 79.
(15) Vysotsky, Y. B.; Bryantsev, V. S.; Boldyreva, F. L.; Fainerman, V. B.; Vollhardt, D. *J. Phys. Chem. B* **2005**, *109*, 454.
(16) Hyperchem, 6th ed.; Hypercube, Inc.: USA, 1999.
(17) Davies, J. T.; Rideal, E. K. *Interfacial Phenomena*, 2nd ed.; Academic Press, Inc.: New York, 1963.
(18) Weers, J. G.; Scheuing, D. R. *Fourier Transform Infrared Spectroscopy in Colloid and Interface Science*; American Chemical Society: Washington, DC, 1991.
(19) Ulman, A. *An Introduction to Ultrathin Organic Films from Langmuir−Blodgett to Self Assembly*; Academic Press: San Diego, 1991.
(20) Byrd, H.; Whipps, S.; Pike, J. K.; Ma, J.; Nagler, S. E.; Talham, D. R. *J. Am. Chem. Soc.* **1994**, *116*, 295.
(21) Taniike, K.; Matsumoto, T.; Sato, T.; Ozaki, Y.; Nakashima, K.; Iriyama, K. *J. Phys. Chem.* **1996**, *100*, 15508.
(22) Yong, H.; Penner, T. L.; Whitten, D. G. *Langmuir* **1994**, *10*, 2757.
(23) Rabolt, J. F.; Burns, F. C.; Schlotter, N. E.; Swalen, J. D. *J. Chem. Phys.* **1983**, *78*, 946.
(24) Zhao, B.; Li, H.; Zhang, X.; Shen, J.; Ozaki, Y. *J. Phys. Chem. B* **1998**, *102*, 6515.
(25) Katayama, N.; Enomoto, S.; Sato, T.; Ozaki, Y.; Kuramoto, N. *J. Phys. Chem.* **1993**, *97*, 6880.
(26) Tang, X. Y.; Schneider, T.; Buttry, D. A. *Langmuir* **1994**, *10*, 2235−2240.
(27) Alves, C. A.; Porter, M. D. *Langmuir* **1993**, *9*, 3507.
(28) Tao, Y. T. *J. Am. Chem. Soc.* **1993**, *115*, 4350.
(29) Neumann, V.; Gericke, A.; Hühnerfuss, H. *Langmuir* **1995**, *11*, 2206.
(30) Snyder, R. G.; Strauss, H. L.; Elliger, C. A. *J. Phys. Chem.* **1982**, *86*, 5145.
(31) Sinniah, K.; Cheng, J.; Terrettaz, S.; Reutt-Robey, J. E.; Miller, C. J. *J. Phys. Chem.* **1995**, *99*, 14500.
(32) Gao, W.; Dickinson, L.; Grozinger, C.; Morin, F. G.; Reven, L. *Langmuir* **1996**, *12*, 6429.
(33) Ren, Y.; Iimura, K.; Kato, T. *J. Phys. Chem. B* **2002**, *106*, 1327.
(34) Lin-Vien, D.; Colthup, N. B.; Fateley, W. G.; Grasselli, J. G. *Infrared and Raman Charactristic Frequencies of Organic Molecules*; Academic Press Inc.: San Diego, 1991.
(35) Rabolt, J. F.; Russell, T. P.; Twieg, R. J. *Macromolecules* **1984**, *17*, 2786.
(36) Lenk, T. J.; Hallmark, V. M.; Hoffmann, C. L.; Rabolt, J. F.; Castner, D. G.; Erdelen, C.; Ringsdorf, H. *Langmuir* **1994**, *10*, 4610.
(37) Tamada, K.; Nagasawa, J.; Nakanishi, F.; Abe, K.; Hara, M.; Knoll, W.; Ishida, T.; Fukushima, H.; Miyashita, S.; Usui, T.; Koini, T.; Lee, T. R. *Thin Solid Films* **1998**, *329*, 150.
(38) Naselli, C.; Swalen, J. D.; Rabolt, J. F. *J. Chem. Phys.* **1989**, *90*, 3855.
(39) Vandevyver, M.; Barraud, A.; Ruaudel-Teixier, A.; Maillard, P.; Gianotti, C. *J. Colloid Interface Sci.* **1982**, *85*, 571.
(40) Miguel, G.; Pedrosa, J. M.; Matín-Romero, M. T.; Muñoz, E.; Richardson, T. H.; Camacho, L. *J. Phys. Chem. B* **2005**, *109*, 3998.
(41) Bunn, C. W.; Howell, E. R. *Nature* **1954**, *174*, 549.
(42) Alloway, D. M.; Hofmann, M.; Smith, D. L.; Gruhn, N. E.; Graham, A. L.; Colorado, R.; Wysocki, V. H.; Lee, T. R.; Lee, P. A.; Armstrong, N. R. *J. Phys. Chem. B* **2003**, *107*, 11690.
(43) El Abed, A.; Ionov, R.; Daoud, M.; Abillon, O. *Phys. Rev. E* **2004**, *70*, 051607.